

# Electronic Properties of Functionalized Diamanes for Field-Emission Displays

Christian Tantardini,\* Alexander G. Kvashnin,\* Maryam Azizi, Xavier Gonze,\* Carlo Gatti, Tariq Altalhi, and Boris I. Yakobson\*



Cite This: *ACS Appl. Mater. Interfaces* 2023, 15, 16317–16326



Read Online

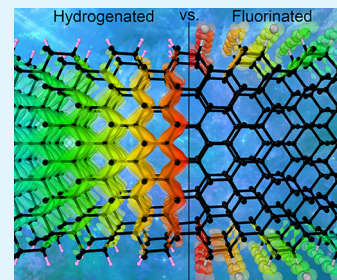
ACCESS |

Metrics & More

Article Recommendations

Supporting Information

**ABSTRACT:** Ultrathin diamond films, or diamanes, are promising quasi-2D materials that are characterized by high stiffness, extreme wear resistance, high thermal conductivity, and chemical stability. Surface functionalization of multilayer graphene with different stackings of layers could be an interesting opportunity to induce proper electronic properties into diamanes. Combination of these electronic properties together with extraordinary mechanical ones will lead to their applications as field-emission displays substituting original devices with light-emitting diodes or organic light-emitting diodes. In the present study, we focus on the electronic properties of fluorinated and hydrogenated diamanes with (111), (110), (0001), (10 $\bar{1}$ ), and (2110) crystallographic orientations of surfaces of various thicknesses by using first-principles calculations and Bader analysis of electron density. We see that fluorine induces an occupied surface electronic state, while hydrogen modifies the occupied bulk state and also induces unoccupied surface states. Furthermore, a lower number of layers is necessary for hydrogenated diamanes to achieve the convergence of the work function in comparison with fluorinated diamanes, with the exception of fluorinated (110) and (2110) films that achieve rapid convergence and have the same behavior as other hydrogenated surfaces. This induces a modification of the work function with an increase of the number of layers that makes hydrogenated (2110) diamanes the most suitable surface for field-emission displays, better than the fluorinated counterparts. In addition, a quasi-quantitative descriptor of surface dipole moment based on the Tantardini–Oganov electronegativity scale is introduced as the average of bond dipole moments between the surface atoms. This new fundamental descriptor is capable of predicting a priori the bond dipole moment and may be considered as a new useful feature for crystal structure prediction based on artificial intelligence.



**KEYWORDS:** diamanes, ABINIT, meta-GGA, GW approximation, Bader theory, Tantardini–Oganov electronegativity, field-emission displays

## INTRODUCTION

Nowadays, the possibilities of applications of two-dimensional materials for electronic devices are scrutinized by numerous research groups worldwide. The search for new materials for application in field-emission displays (FEDs) represents a very hot topic due to the necessity to produce flatter panels (i.e., approximately 2 mm) with the characteristics of self-emissive distortion-free images and wide view angles (i.e., about 170°). Furthermore, FEDs are characterized by quick response, in the order of microseconds, tolerance to environments as high as that of receiving tubes, and free from terrestrial and applied magnetic effects.<sup>1–6</sup> These characteristics make FEDs more appreciated than corresponding light-emitting diodes (LEDs), organic light-emitting diodes (OLEDs), and surface-conduction electron-emitter displays (SEDs).<sup>1–6</sup> The search for new materials employed as FEDs benefits enormously from a deep study of the electronic structure at the surface, which in most cases is peculiar and differs from the bulk, due to the significantly changed chemistry caused by the surface-modified bonding pattern.

Considering carbon materials, one notes that diamond and lonsdaleite are both sp<sup>3</sup>-hybridized insulating allotropes, while their 2D counterpart graphene<sup>7,8</sup> is a semimetal with sp<sup>2</sup>-hybridized carbon atoms. Indeed, the hybridization plays an important role not only in the chemistry but also in the electronic properties of carbon materials. In particular, the surface functionalization of multilayer graphene with different stackings of layers by different atoms enables chemically induced phase transition converting multilayer graphene into diamond-type structures with sp<sup>3</sup>-hybridized carbon atoms in all layers leading to semiconducting properties.<sup>9–17</sup> These functionalized multilayers are different from graphene that presents sp<sup>2</sup> hybridization of carbons and electronic properties of a semimetal. The sp<sup>3</sup>-hybridized multilayers are quasi-2D

Received: February 2, 2023

Accepted: March 7, 2023

Published: March 16, 2023



compounds called diamanes, various structures of which are caused by AA, AA', or AB stackings of graphene layers.<sup>9,11–17</sup> More exotic structures can be formed by fabrication of moiré patterns from bilayer graphene functionalized by hydrogen or fluorine,<sup>16,18–22</sup> and even quasicrystals can be formed.<sup>23</sup>

Indeed, the formation of diamanes from multilayer graphene via the application of low temperature and pressure ( $\sim 50$  Torr) was observed experimentally in refs.<sup>24,25</sup> Authors applied the hot-filament process for the efficient hydrogenation and dehydrogenation of few-layered graphene and the subsequent formation of crystalline and ultrathin  $sp^3$  carbon sheets observed.

Diamanes exhibit a unique combination of physical properties such as high thermal conductivity,<sup>26–31</sup> which is compatible with small-polaron charge carriers, and optical characteristics,<sup>32–34</sup> making them suitable for potential applications in electromechanical devices.<sup>30</sup> In addition, diamanes with different functionalizations of surfaces could be good candidates for FEDs. Indeed, 2D materials are also remarkable due to the possibility of doping their surface in a reversible way by functionalization/defunctionalization. Hence, the switching of electronic properties from metals to semiconductors and vice versa occurs due to the chemical or photochemical reactions. A sort of reversible photodoping was recently discovered by Gierster et al.<sup>35</sup> at the  $(10\bar{1}0)$  surface of ZnO, where phase transition is caused by photoinduced downward surface band bending due to photodepletion of donor-type deep surface defects.

Hydrogenated diamanes are a case of reversible chemical doping.<sup>24,36–39</sup> Furthermore, reversible fluorination of few-layer graphene was also experimentally achieved in refs.<sup>40–43</sup> Actually, for both hydrogenated and fluorinated diamanes, the energy barrier of hydrogenation or fluorination decreases with the number of layers and the monolayer is the most difficult structure to be formed from this point of view.<sup>13,14,44</sup>

Thus, to understand the possibility of using diamanes in FEDs, a state-of-the-art fundamental study of their electronic properties with first-principles calculations is much needed, which is the goal of the present work. Indeed, the Kohn–Sham (KS) electronic band structure together with  $GW$  approximation gap values<sup>45</sup> allow us to understand the dependence of the work function on the functionalization type and thickness of diamanes. A subsequent study of electron population at the valence band maxima (VBM) within the framework of Bader theory<sup>46,47</sup> applied for 2D materials<sup>48,49</sup> enables us to understand the atomic contribution responsible for the conductivity, making clear the electronic transport behavior at the atomic level in view of the future development of 2D optoelectronic devices based on diamanes.

## RESULTS AND DISCUSSION

Five types of diamanes are considered, having (111), (110), (0001),  $(10\bar{1}0)$ , and  $(\bar{2}110)$  crystallographic orientations of surfaces, with thickness from 1 to 6 layers and hydrogen or fluorine functionalization, so altogether 60 structures. Hydrogen and fluorine atoms are bonded with the surface carbon atoms through a covalent bonds. Thus, all carbon atoms in the considered diamanes are  $sp^3$ -hybridized. Atomic structures of these five types of diamanes are shown in Figure 1. Diamanes with (111) and (110) surfaces belong to a group of films with the cubic diamond structure type, while other films have the lonsdaleite (hexagonal diamond) structure type. Yellow atoms in Figure 1 represent noncarbon atoms (hydrogen or fluorine,

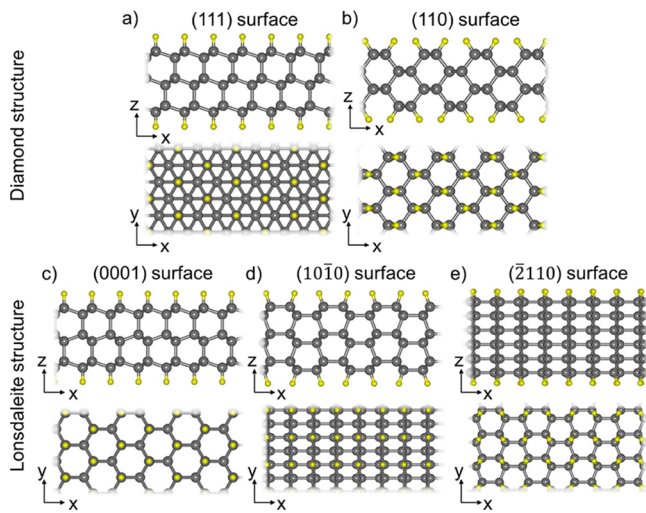


**Figure 1.** Top and side views of atomic structures of the considered diamanes with diamond and lonsdaleite structures having (a) (111), (b) (110), (c) (0001), (d)  $(10\bar{1}0)$ , and (e)  $(\bar{2}110)$  surfaces respectively. Gray balls represent carbon atoms and yellow balls are noncarbon atoms (H or F).

which are presented here). Films with (0001) and  $(\bar{2}110)$  surfaces can be formed by passivation of graphene multilayers with AA stacking, while AA' stacking leads to formation of  $(10\bar{1}0)$  films.<sup>12</sup>

For each considered diamane, the KS electronic band structure is calculated by using the TB09 (aka modified Becke–Johnson, a meta-generalized gradient approximation (GGA) functional) DFT exchange-correlation functional<sup>50</sup> on top of a GGA-PBE optimized structure, as shown in Figures S1–S10 in the Supporting Information. The TB09 functional is quite efficient in calculating the accurate band gap of various bulk materials, with respect to LDA and GGA-PBE, and is in a reasonable agreement with the  $GW$  approximation or experimental data for bulk solids.<sup>50–52</sup> This makes it a priori an excellent starting point to achieve useful information about electronic band structures and band gaps for 3D structures<sup>53</sup> and we will test it here on 2D structures.

All hydrogenated (111), (110), (0001),  $(10\bar{1}0)$ , and  $(\bar{2}110)$  diamanes possess direct TB09 KS band gaps (Figures S1–S10 in the Supporting Information). Few-layer fluorinated (111), (110), (0001), and  $(10\bar{1}0)$  diamanes are characterized by direct band gaps, while an increase in thickness leads to the appearance of an indirect band gap, with the exception of  $(\bar{2}110)$ , which is a direct gap semiconductor for all considered thicknesses (Figures S1–S10 in the Supporting Information). As we know, the band gap analysis gives a crucial information about the system. However, the accuracy of the KS electronic band structure is affected by the DFT problem that underestimates the band gap and overestimates the electronic repulsion with the Hartree term that is not always properly balanced with the exchange-correlation functional.

To evaluate the quantitative prediction of band gaps in 2D solids obtained with TB09, we have subsequently performed  $G_0W_0$  calculations on top of the TB09 DFT results (from now on, referred to as  $GW@TB09$ ). Furthermore, we have compared fundamental and direct gaps obtained with  $GW@TB09$  as a function of the inverse squared number of layers (see Figures 2 and S11 in the Supporting Information). This was done according to the fact that in quantum mechanics, the

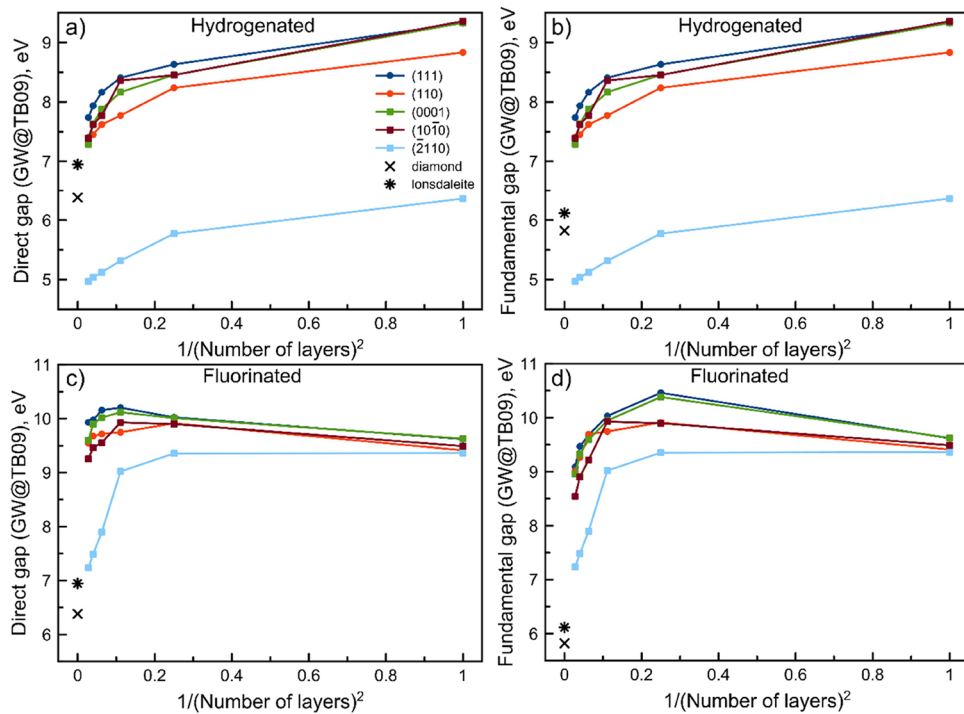


**Figure 2.** Dependency on the squared inverse number of layers (thickness) of the direct (a, c) and fundamental (b, d) band gaps for hydrogenated (a, b) and fluorinated (c, d) diamanes, calculated by the *GW*@TB09 approach.

energy level spacing of a particle in a square box (like a confined electron) is a function of the inverse squared box size. Theoretically, an increase in the number of layers ( $L$ ) of diamanes should lead to a decrease in the band gap until converging to the value for bulk lonsdaleite or diamond in the limit of  $L \rightarrow \infty$ . In reality, such behavior is preserved for bulk states, but modifications do not follow the same law for surface state(s).

Moreover, comparing the *GW*@TB09 (see Figure 2) with TB09 (see Figure S11 in the Supporting Information) band gap dependencies, we observe two totally different behaviors. Both fundamental and direct band gaps of all hydrogenated diamanes calculated by TB09 decrease with the increase of the number of layers and starting from three layers, band gaps start to increase, Figure S11a,b. Fluorinated films demonstrate nonmonotonic behavior of band gaps with thickness (Figure S11c,d). Interestingly, this band gap behavior of (2110) diamanes is counterintuitive, namely, there is no tendency to the band gaps of bulk lonsdaleite with  $L \rightarrow \infty$ . More accurate *GW*@TB09 corrects this situation, as shown in Figure 2. In order to double-check our *GW*@TB09 predictions, we examined whether there might be a reordering of electronic bands calculated by TB09 and  $G_0W_0$  that might change the electronic states in hydrogenated (111), (110), (0001), (1010), and (2110) diamanes at the band gap extrema. We have monitored the energy difference between the bands at VBM with respect to the closest highest bands, confirming that no reordering occurs. Thus, while TB09 is considered as one of the best choices for the KS band structure for 3D materials,<sup>53</sup> for 2D systems, its predictive capability seems degraded.

From our *GW*@TB09 results (see Figure 2), the increase of the number of layers in hydrogenated diamanes always induces a decrease of the band gap from its initial value (monolayer, graphane). At variance, in fluorinated diamanes, the band gap is seen to initially increase with the number of layers from the

monolayer and subsequently decrease after three layers, to converge, in the larger thickness, to the corresponding band gap of the bulk counterpart. Furthermore, only hydrogenated (2110) films display a clear band gap behavior that does not converge to the band gap of lonsdaleite with the increase of the number of layers (blue curves in Figure 2).

The band gap behavior is affected by different functionalizations of the surfaces, which are correlated with the electronic states. This can be understood by looking at the KS electronic band structures (Figures S1–S10 in the Supporting Information) that are not affected by reordering, as was checked previously with *GW* calculations. KS TB09 electronic band structures (see in Supporting Information Figures S1–S10) are intricate and benefit from further investigation using Bader theory.

Bulk electronic states in such multilayers are characterized by the Bloch character of the wavefunction in the inner layers while decaying exponentially into a vacuum. Instead, surface electronic states are characterized by exponential decay both in vacuum and in the inner layers and thus represents states localized at the crystal surface.

These two types of states, from the occupied bulk valence states and from the occupied surface states, contribute to the charge density of the bulk and surface with different atomic characteristics.

Actually, in the presence of a few layers, it is difficult to speak about localized surface electronic states, because the whole few-layer structure is made of the surface. Thus, the localization can come only in the presence of thicker multilayers. Thus, we can suppose that the different band gap behaviors for fluorinated and hydrogenated diamanes with the increase of layers are due to the formation of surface electronic states in one case and due to bulk electronic states in the other.

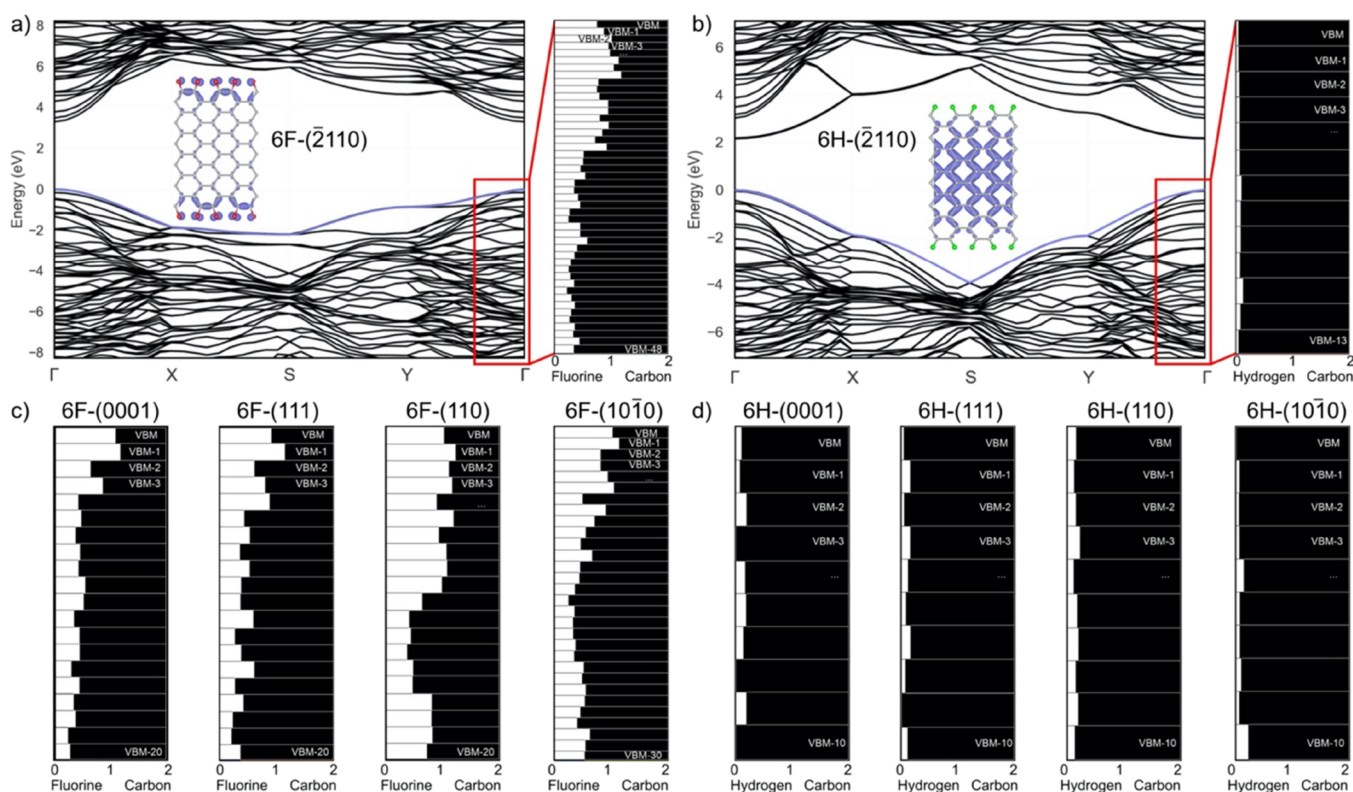


**Figure 3.** Electronic band structures of six-layer ( $\bar{2}110$ ) diamanes functionalized by (a) fluorine and (b) hydrogen, calculated with TB09. The insets show the charge density isosurface of electrons localized at the VBM. The isosurface value for the fluorinated diamane is  $0.0068 \text{ e}/\text{\AA}^3$ ; for the hydrogenated diamane, the isosurface value is  $0.0045 \text{ e}/\text{\AA}^3$ . The electronic band colored in blue corresponds to the VBM for which the charge density is plotted for both fluorinated and hydrogenated diamanes. The right panels show the ratio of atomic population of fluorine/hydrogen and carbon atoms from the VBM to lower bands. Similar plots are shown for the atomic population for the other crystallographic orientations (111), (110), (0001), and ( $10\bar{1}0$ ) of (c) fluorinated and (d) hydrogenated diamanes from the VBM to the lower bands.

Two different electronic states can be recognized by different electronic atomic contribution to the VBM: an electronic atomic contribution coming from all bulk atoms is responsible for a bulk state; an electronic contribution coming for specific localized atoms is responsible for a surface electronic state. This can be quantified through a Bader analysis.

In the case of surface electronic states, the charge density at the VBM might come from surface adatoms, as well as from the carbon atoms adjacent to these. The latter is responsible for the variation of electronic distribution within the multilayer with a conductivity that does not depend on the excitation of electrons from the surface adatoms.

Hence, Bader theory<sup>46</sup> provides a detailed characterization of the surface and bulk electronic states in diamanes with different functionalizations and provides a partition of charge in different atomic contributions. In such theory (also called QTAIM, i.e., quantum theory of atoms in molecules),<sup>46</sup> the atoms are not considered as spherical units intrinsically defined and independent by the context, but their shape and volume are strongly influenced by the surrounding atoms. Atoms in molecules are defined as atomic basins delimited by the so-called zero-flux surface. Such surface is made by the infinity of points  $r$ , for which the dot product of the gradient of electron density,  $\nabla\rho$ , and the normal vector to the surface,  $\hat{n}$ , is zero (zero-flux boundary condition,  $\nabla\rho(r) \cdot \hat{n}(r) = 0$ ). We have calculated the charge density at the VBM and integrated such density within Bader atomic basins bounded by zero-flux surfaces calculated with the full electron density.<sup>46</sup> This was

done for the six-layer diamanes. It is seen that hydrogenated diamane states, close to the top of the valence band, are predominantly bulk electronic states, while fluorinated diamanes possess important localized surface electronic states, see Figures 3, S12, and Table S15 in the Supporting Information.

Let us have now a look in detail at the diamane with the ( $\bar{2}110$ ) surface (Figure 3), which is the characteristic multilayer showing two different band gap behaviors as a function of the functionalization type (fluorine or hydrogen). As can be seen by the KS band structures in Figure 3a,b, where the electronic band structures calculated by TB09 are shown: bulk and surface electronic states are observed for hydrogenated and fluorinated diamanes respectively.

Now, we explain in detail the fluorinated (Figure 3a) and hydrogenated diamanes with ( $\bar{2}110$ ) surfaces (Figure 3b) to rationalize the correlation between the KS electronic band structure and the band population from the VBM to the inner bands.

The KS electronic band structures of fluorinated diamanes (Figures S2, S4, S6, S8, and S10 in the Supporting Information) show surface electronic states that are supported by the population of VBM and first-inner bands are characterized by surface fluorine atoms and their bonded carbon atoms (Figure 3a). As we look in deeper bands, the contribution of carbon atoms to the electronic population becomes predominant (Figure 3a). The same kind of band population is shown by the Bader analysis for the other structures (Figure 3c).

The KS electronic band structures of hydrogenated diamanes (Figures S1, S3, S5, S7, and S9 in the Supporting Information) show bulk electronic states that are supported by spreading of hydrogen atomic charge density into the inner bands with a charge density at the VBM dominated by the atomic charge density of carbon atoms as shown in Figure 3b,d.

The  $(\bar{2}110)$  hydrogenated diamane shows a pronounced difference between conduction band minima (CBM) and the first closest higher conduction band. This is responsible for such different band gap behaviors as seen in Figure 2 with respect to the hydrogenated diamanes with other surfaces showing a similar energy difference between CBM and the higher conduction bands.

As the difference between surface and bulk states at band edges affects the properties at the surface in different ways, we have calculated the work function from PBE (see Supporting Information Figure S13 and Table S13) and  $GW@PBE$  (see Figure 4 and Supporting Information Table S13), depending on the number of layers, to understand how many layers are necessary to obtain a promising FED.

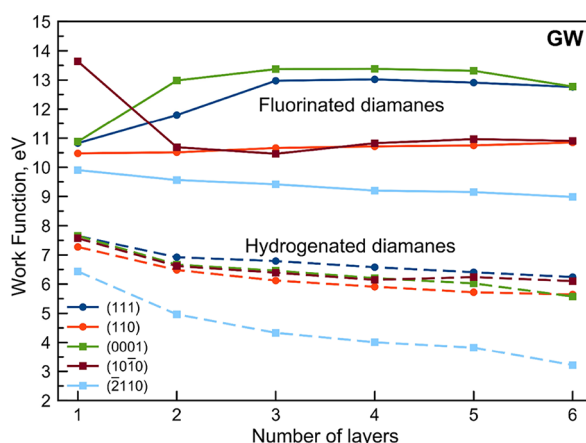


**Figure 4.** Work function depending on the number of layers for the considered fluorinated and hydrogenated diamanes with different orientations of surfaces obtained by  $GW@PBE$ .

Indeed, we have observed a different work function behavior after  $GW$  correction that significantly shifts the VBM with respect to PBE results as expected for the band gap results obtained with  $GW$  correction on top of TB09.

The work function values of fluorinated diamanes are larger than that of hydrogenated ones and linearly decreases except for (111) and (0001) surfaces where the work function displays a behavior similar to the band gap dependence, namely, the work function increases from the monolayer to three layers and then decreases. This is coherent with the formation of local surface states in the case of multilayers, which for such structure also affects the work function behavior. Furthermore, the F-(2110) diamanes have the same behavior as H-(111), H-(110), H-(0001), and H-(1010) films, although having a higher work function than hydrogenated ones for thin films, see Figure 4. It monotonically decreases with the increase of the number of layers, reaching  $\sim 6$  eV at six layers.

The  $GW$  correction singles out the hydrogenated  $(\bar{2}110)$  surface that has the lowest work function values, starting from

$\sim 6.5$  eV for the monolayer, decreasing with the number of layers, and achieving  $\sim 3.5$  eV for six layers.

An additional concept that we analyzed in our work is the dipole moment in 2D materials to understand the intrinsic electronic properties of diamanes. Usually, in 2D materials one evaluates the surface dipole moment, which describes the transfer of charge that happens at the interface between the edge of the material and vacuum when a fictitious potential is applied. To describe the charge distribution at the surface, different models were previously developed: the Helmholtz model, where an electric double layer consisting of two oppositely charged layers is assumed and where the charges on the surface of the material form a pearl necklace (i.e., uniform distribution) where charges are free to move;<sup>54</sup> the Gouy–Chapman model, where the interfacial potential is created like in the Helmholtz model, with the difference that the charges in vacuum are not free to move and are in the same number and opposite in sign to those of the surface of the material;<sup>55,56</sup> and the Stern model, which suggests a hybrid model between the two previously described, with ions that have finite size, so they cannot approach the surface closer than a few nanometers.<sup>57</sup>

Unfortunately, these classical models fail to describe the experimental data and cannot describe the formation of dipole moments at the interface. Furthermore, these kinds of models do not deliver any intrinsic information about the electronic properties of materials.

Now, if we focus on the effects on the electronic properties simply due to the functionalization of the surfaces of diamanes, then the chemical bonding between carbon and surface adatoms will be characterized by the formation of a bond dipole moment, whose intensity depends on the different electronegativities of elements. These bond dipole moments appearing between carbon and surface adatoms will be responsible for the charge separation at the surface of the film determining the intrinsic electronic properties of that functionalized material. Thus, the direction of each bond dipole moment at the surface will characterize the chemical properties of the material at the atomistic level. If a bond dipole moment between carbon and surface adatoms is directed toward the deep layers or out from the material, then the electron affinity of the surface will change together with the chemical reactivity.

Hence, as we know, the bond dipole moment is defined as<sup>58</sup>

$$\mu_D = \delta d \quad (1)$$

where  $\delta$  is the difference between the partial charges of bounded atoms,  $\delta = \delta^+ - \delta^-$ ,  $d$  is the bond length in angstroms.

The problem with this historical definition stems from the estimation of atomic partial charges. At present, such estimation relies on using first-principles calculations that are nontrivial due to the self-interaction error and requires complex calculations within constrained DFT<sup>59–61</sup> and the kind of chosen atomic partition can also be a source of errors as underestimation or overestimation.<sup>60</sup> It would be desirable to determine the bond dipole moments *a priori* from a simpler perspective, in order to predict more straightforwardly new functionalized multilayers with desired characteristics that strictly depend on the electron density distribution at the surface.

Thus, we have tested the possibility to correlate the difference between the electronegativities of two atoms,  $\Delta X_{AB}$ , with their supposed bond dipole moment. Here, we

**Table 1.** Bond Length, Electronegativity Difference, Calculated and Measured Dipole Moment for Several Molecules with Hydrogen<sup>a</sup>

diatomic molecule	$d_A$	$\Delta X_{AB}$	$\mu_{TO}$	$\mu_D/(D)$	$\mu_{wf}/(D)$	$\mu_{Bader}(CC)/(D)$	$\mu_{Bader}(\text{VASP})/(D)$ <sup>62</sup>
HF	0.9200	0.96	1.67	1.82 <sup>63</sup>	1.93	3.56	3.18 <sup>62</sup>
HCl	1.2700	0.5	1.20	1.08 <sup>63</sup>	1.19	1.95	2.32 <sup>62</sup>
HBr	1.4100	0.41	1.09	0.82 <sup>63</sup>	0.89	1.15	2.84 <sup>62</sup>
HI	1.6100	0.16	0.49	0.44 <sup>63</sup>	0.52	0.85	3.40 <sup>62</sup>

<sup>a</sup> $\mu_{Bader}(\text{CC})$  is calculated in this work, while  $\mu_{Bader}(\text{VASP})$  is from ref 62.

have looked for a correlation between the  $\Delta X_{AB}$  coming from the Tantardini–Oganov<sup>62</sup> thermochemical electronegativity scale and bond dipole moment. We estimate the bond dipole moment in terms of  $\Delta X_{AB}$  as:

$$\mu_{TO} = \Delta X_{AB} \cdot \left( \frac{d_A}{a_0} \right) \quad (2)$$

where  $\Delta X_{AB}$  is multiplied by the bond distance in angstroms,  $d_A$ , and divided by the Bohr radius,  $a_0$ , in angstroms, which is equal to 0.529177 Å. This allows us to use dimensionless values for bond dipole moments.

We have tested our formula on molecules containing hydrogen atoms to see if our approach is applicable. Since we selected only neutral diatomic molecules, where  $\delta^+$  is by nature equal to  $-\delta^-$ , and the estimated bond dipoles  $\mu_{TO}$  may be rigorously compared with the experimental or calculated dipole moments. The latter, obtained from the calculated wavefunction as an average of the  $r$  operator, may be also roughly estimated using atomic charges obtained from the same wavefunction and using some basis set or real space partition criterion. Results shown in Table 1 confirm our suggestion to use  $\mu_{TO}$  as a semiquantitative predictor for (bond) dipole moment.

The value of  $\mu_{TO}$  is seen within 10–30% of those taken from the NIST database<sup>63</sup> corresponding to experimental measured values in debye,  $\mu_D$ , and within 10–20% of those obtained from our coupled cluster wavefunction calculations ( $\mu_{wf}$ ) using single, double, and triple excitations and a triple  $\zeta$  local basis set. Dipole moments simply approximated from Bader charges with a plane wave basis set in the VASP package ( $\mu_{Bader}(\text{VASP})$ ) from ref 62) greatly overestimate the experimental ones. Though a bit closer to the NIST database values, the dipole moments calculated from Bader charges obtained from the coupled cluster wavefunction are much larger than both those from the experiment and those calculated directly from the wavefunction. This is not at all surprising since to reconstruct exactly the wavefunction dipole moment, one has to add to the considered charge transfer contribution also that due to the atomic dipoles that in the case of systems with large ionic character is opposite in sign and of the same order of magnitude as the charge transfer contribution.<sup>64,65</sup>

It is noteworthy that it is possible to introduce a “semiquantitative” instrument to determine a priori the bond dipole moment by simply using a pen and paper with Tantardini–Oganov electronegativity without complex quantum chemical calculations.

Thus, by simply knowing the geometry of the system and the difference of electronegativity between two bound atoms, it is possible to define their bond dipole moment. In fact, the distance between two bound atoms assumes the meaning of weight of electronic cloud distribution between two atoms.

We have then estimated  $\mu_{TO}$  between carbon and hydrogen/fluorine atoms for our diamanes, showing that in case of surface and bulk states for hydrogenated and fluorinated diamanes, respectively, the dipole moment does not change with increasing the number of layers (see Tables S11 and S12 in the Supporting Information). However, if we define the surface dipole moment as the average of  $\mu_{TO}$  between the adatoms of the surface and the surface carbon atoms, then we can describe the polarization at the surface after functionalization.

Here, we observed that the average of  $\mu_{TO}$  is ~2.5 for all fluorinated diamanes, while it is only ~0.2 for hydrogenated ones. The strongest dipole moment present on the fluorinated diamane surfaces can be also considered responsible for the linear behavior of the work function and in the observed range, the saturation is not achieved. Nevertheless, the lowest surface dipole moment of hydrogenated diamanes allows them to achieve faster saturation, making them a better candidate for FEDs.

## CONCLUSIONS

Our first-principles investigation of the direct and fundamental band gaps of hydrogenated and fluorinated diamanes, which represent two successful cases of reversible chemical doping, showed a behavior compatible with the formation of occupied surface electronic states for hydrogenated diamanes but no such surface states for fluorinated diamanes were observed. The Bader analysis allowed us to corroborate this view through the study of the electronic population at the VBM. The nature of band gap behavior is responsible for the changes of the work function, namely, bulk electronic states in hydrogenated diamanes are correlated with the small values of the work function that rapidly saturates with the increase of the number of layers, while surface electronic states in fluorinated diamanes deliver a large work function that is also observed to decrease slowly with increasing the number of layers with the exception of fluorinated (110) and (2̄110). It is noteworthy that H-(2̄110) is the most suitable surface for FEDs. We have also been able to correlate the Tantardini–Oganov electronegativity scale with the bond dipole moment showing the extension of such an approach to condensed matters and envisaging the possibility to avoid expensive first-principles calculations and a priori making a prediction on surface reactivity.

## METHODS

**Computational Details.** Structure relaxations and total energy calculations were performed using the optimized norm-conserving Vanderbilt pseudopotentials (ONCVP)<sup>66,67</sup> and the GGA with the Perdew–Burke–Ernzerhof (PBE) exchange-correlation density functional<sup>68</sup> as implemented in ABINIT ver. 9.0.4.<sup>69,70</sup> ONCVP were adopted with 4, 1, and 7 valence electrons for carbon, hydrogen, and fluorine atoms, respectively. The geometry optimization relies on the

Broyden–Fletcher–Goldfarb–Shanno (BFGS)<sup>71–74</sup> algorithm with a convergence cutoff of  $5.0 \times 10^{-5}$  Ha/bohr for the maximum net force on atoms, while the self-consistent field convergence criteria is based on a residual potential cutoff equal to  $10^{-12}$  Ha. A plane wave energy cutoff of 50 Ha and Fermi–Dirac smearing of electronic occupations equal to 0.001 Ha ensure the convergence of total energies. The  $\Gamma$ -centered  $k$ -point meshes of  $6 \times 6 \times 1$  for diamanes and  $6 \times 6 \times 6$  for bulk diamond and lonsdaleite were used for the first Brillouin zone sampling.

$G_0W_0$  and KS electronic band structure calculations were performed with norm-conserving relativistic separable dual-space Gaussian pseudopotentials (HGH),<sup>75</sup> having the same number of valence electrons adopted in the ONCVP. KS electronic structures were calculated using TB09 and PBE exchange-correlation functionals.<sup>50</sup> For  $G_0W_0$  calculations, the number of unoccupied bands per atom is 50 and the energy cutoff for the dielectric matrix is 5 Ha, which guarantees a band gap convergence in the order of 2 meV.  $G_0W_0$  calculations for the multilayers were performed considering the Coulomb singularity problem that happens at  $G = 0$  and that hinders the convergence with respect to the number of  $k$ -points used to sample the first Brillouin zone, thanks to the Ismail-Beigi methodology.<sup>76</sup> These calculations were performed considering the degeneracy of bands at the VBM and CBM looking for the  $GW@$  TB09 band gap as the difference between the two degenerate bands at VBM and the two degenerate bands at the CBM.

No attempt was made to perform self-consistent  $GW$  calculations. Instead, calculations relied on the DFT electronic charge densities throughout. The electronic charge density change from such self-consistent  $GW$  with respect to the DFT one is not large anyhow, the variation being in the order of a millielectron per atomic unit, as reported in ref 77. Thus, electronic charge densities at the VBM showed throughout are KS TB09 ones.

The planewave-based multilayer calculations, with an inherent artificial periodicity perpendicular to the multilayer, were performed without adding a planar dipole layer in the vacuum region,<sup>78</sup> because all the slabs are hydrogenated (or fluorinated) on both sides of the slab, equally, so, their surface dipole long-range effects cancel each other and there is no long-range buildup of the electric field due to these surface dipoles in the ground-state.

The work function was determined as the difference of energy between the highest occupied state and the vacuum level, the latter obtained by the macroscopic average technique of Baldereschi et al.<sup>79</sup> The highest state energy was the one from  $GW@PBE$  calculation, following the so-called  $GW$ -VBM approach, see eq 3 of ref 80. Results were compared with the uncorrected PBE values in the Supporting Information.

The electronic charge density for test molecules (see Table 1) was calculated with coupled cluster single, double, and triple excitations using Gaussian local basis sets aug-cc-pVTZ (all-electron triple  $\zeta$  basis set with diffusive and polarized) for hydrogen, fluorine, and chlorine atoms,<sup>81</sup> while aug-cc-pwCVTZ-PP (relativistic triple  $\zeta$  basis set with diffusive and polarized) was used for bromine and iodine atoms.<sup>82,83</sup> Their molecular geometries were taken from experimental data<sup>63</sup> and are shown in the Table 1 of the main text together with experimental dipole moments. The threshold energy of SC convergence was chosen to be  $10^{-8}$  Ha.

All first-principles and quasiparticle calculations on solids were performed with ABINIT.<sup>69,70</sup> The post-Hartree–Fock calculations on molecules were performed using Gaussian G16 version<sup>84</sup> The Bader analysis was performed using the CRITIC2 program.<sup>85</sup> The crystal structures were visualized using VESTA software.<sup>86</sup>

## ASSOCIATED CONTENT

### Supporting Information

The Supporting Information is available free of charge at <https://pubs.acs.org/doi/10.1021/acsami.3c01536>.

It contains details of the atomic structure of the studied diamanes films, the electronic band structures, the dependency of direct and fundamental band gaps as a

function of the layer thickness, calculated by using the TB09 approach, and the charge density coming from various atomic basins at the valence band maximum and inner bands ([PDF](#))

## AUTHOR INFORMATION

### Corresponding Authors

Christian Tantardini – Hylleraas Center, Department of Chemistry, UiT The Arctic University of Norway, N-9037 Tromsø, Norway; Department of Materials Science and NanoEngineering, Rice University, Houston, Texas 77005, United States; Institute of Solid State Chemistry and Mechanochemistry SB RAS, Novosibirsk 630128, Russian Federation; [orcid.org/0000-0002-2412-9859](#); Email: [christiantantardini@gmail.com](mailto:christiantantardini@gmail.com)

Alexander G. Kvashnin – Skolkovo Institute of Science and Technology, Moscow 121205, Russian Federation; [orcid.org/0000-0002-0718-6691](#); Email: [a.kvashnin@skoltech.ru](mailto:a.kvashnin@skoltech.ru)

Xavier Gonze – Université catholique de Louvain, Ottignies-Louvain-la-Neuve 1348, Belgium; [orcid.org/0000-0002-8377-6829](#); Email: [xavier.gonze@uclouvain.be](mailto:xavier.gonze@uclouvain.be)

Boris I. Yakobson – Department of Materials Science and NanoEngineering, Rice University, Houston, Texas 77005, United States; Chemistry Department, Taif University, Taif 26571, Saudi Arabia; [orcid.org/0000-0001-8369-3567](#); Email: [biy@rice.edu](mailto:biy@rice.edu)

### Authors

Maryam Azizi – Université catholique de Louvain, Ottignies-Louvain-la-Neuve 1348, Belgium

Carlo Gatti – SCITEC - Istituto di Scienze e Tecnologie Chimiche "Giulio Natta", CNR - Consiglio Nazionale delle Ricerche, Milan 20133, Italy

Tariq Altalhi – Chemistry Department, Taif University, Taif 26571, Saudi Arabia

Complete contact information is available at: <https://pubs.acs.org/10.1021/acsami.3c01536>

### Notes

The authors declare no competing financial interest.

## ACKNOWLEDGMENTS

The authors thank Alberto Otero-de-la-Roza from the University of Oviedo, Davide Ceresoli from CNR-SCITEC Milano, and Matteo Giantomassi from UCLouvain for useful discussion. This work has been supported by the Federal Government of Belgium through the EoS Project ID 40007525, and the NOMAD2, INFRAEDI-05-2020 Integrated Infrastructure Initiative funded by the EU HORIZON 2020, Grant Agreement 951786. T.A. and B.I.Y. acknowledge the Taif University Research Support Project (TURSP-HC2022/1, Saudi Arabia). C.T. performed the calculations on resources provided by Sigma2—The National Infrastructure for High Performance Computing Data Storage in Norway.

## REFERENCES

- (1) Awan, T. I.; Bashir, A.; Tehseen, A. *Chemistry of Nanomaterials: Fundamentals and Applications*, 1st edition.; Elsevier: Amsterdam, Netherlands; Cambridge, MA, 2020.
- (2) Talin, A. A.; Dean, K. A.; Jaskie, J. E. *Field Emission Displays: A Critical Review*. *Solid-State Electron.* **2001**, *45*, 963–976.

- (3) Choi, W. B.; Chung, D. S.; Kang, J. H.; Kim, H. Y.; Jin, Y. W.; Han, I. T.; Lee, Y. H.; Jung, J. E.; Lee, N. S.; Park, G. S.; Kim, J. M. Fully Sealed, High-Brightness Carbon-Nanotube Field-Emission Display. *Appl. Phys. Lett.* **1999**, *75*, 3129–3131.
- (4) Kim, J. M.; Choi, W. B.; Lee, N. S.; Jung, J. E. Field Emission from Carbon Nanotubes for Displays. *Diam. Relat. Mater.* **2000**, *9*, 1184–1189.
- (5) Saito, Y.; Uemura, S. Field Emission from Carbon Nanotubes and Its Application to Electron Sources. *Carbon* **2000**, *38*, 169–182.
- (6) Patra, A.; More, M. A.; Late, D. J.; Rout, C. S. Field Emission Applications of Graphene-Analogous Two-Dimensional Materials: Recent Developments and Future Perspectives. *J. Mater. Chem. C* **2021**, *9*, 11059–11078.
- (7) Novoselov, K. S.; Geim, A. K.; Morozov, S. V.; Jiang, D.; Zhang, Y.; Dubonos, S. V.; Grigorieva, I. V.; Firsov, A. A. Electric Field Effect in Atomically Thin Carbon Films. *Science* **2004**, *306*, 666–669.
- (8) Novoselov, K. S.; Andreeva, D. V.; Ren, W.; Shan, G. Graphene and Other Two-Dimensional Materials. *Front. Phys.* **2019**, *14*, 13301.
- (9) Chernozatonskii, L. A.; Sorokin, P. B.; Kvashnin, A. G.; Kvashnin, D. G. Diamond-like C<sub>2</sub>H Nanolayer, Diamane: Simulation of the Structure and Properties. *JETP Lett.* **2009**, *90*, 134–138.
- (10) Chernozatonskii, L. A.; Sorokin, P. B.; Kuzubov, A. A.; Sorokin, B. P.; Kvashnin, A. G.; Kvashnin, D. G.; Avramov, P. V.; Yakobson, B. I. Influence of Size Effect on the Electronic and Elastic Properties of Diamond Films with Nanometer Thickness. *J. Phys. Chem. C* **2011**, *115*, 132–136.
- (11) Sivek, J.; Leenaerts, O.; Partoens, B.; Peeters, F. M. First-Principles Investigation of Bilayer Fluorographene. *J. Phys. Chem. C* **2012**, *116*, 19240–19245.
- (12) Kvashnin, A. G.; Sorokin, P. B. Lonsdaleite Films with Nanometer Thickness. *J. Phys. Chem. Lett.* **2014**, *5*, 541–548.
- (13) Kvashnin, A. G.; Chernozatonskii, L. A.; Yakobson, B. I.; Sorokin, P. B. Phase Diagram of Quasi-Two-Dimensional Carbon, From Graphene to Diamond. *Nano Lett.* **2014**, *14*, 676–681.
- (14) Antipina, L. Y.; Sorokin, P. B. Converting Chemically Functionalized Few-Layer Graphene to Diamond Films: A Computational Study. *J. Phys. Chem. C* **2015**, *119*, 2828–2836.
- (15) Kvashnin, A. G.; Avramov, P. V.; Kvashnin, D. G.; Chernozatonskii, L. A.; Sorokin, P. B. Features of Electronic, Mechanical, and Electromechanical Properties of Fluorinated Diamond Films of Nanometer Thickness. *J. Phys. Chem. C* **2017**, *121*, 28484–28489.
- (16) Chernozatonskii, L. A.; Demin, V. A.; Kvashnin, D. G. Fully Hydrogenated and Fluorinated Bigraphenes–Diamanes: Theoretical and Experimental Studies. *C* **2021**, *7*, 17.
- (17) Sorokin, P. B.; Yakobson, B. I. Two-Dimensional Diamond–Diamane: Current State and Further Prospects. *Nano Lett.* **2021**, *21*, 5475–5484.
- (18) Chernozatonskii, L. A.; Demin, V. A.; Kvashnin, D. G. Ultrawide-Bandgap Moiré Diamanes Based on Bigraphenes with the Twist Angles  $\Theta \sim 30^\circ$ . *Appl. Phys. Lett.* **2020**, *117*, 253104.
- (19) Chernozatonskii, L. A.; Katin, K. P.; Demin, V. A.; Maslov, M. M. Moiré Diamanes Based on the Hydrogenated or Fluorinated Twisted Bigraphene: The Features of Atomic and Electronic Structures, Raman and Infrared Spectra. *Appl. Surf. Sci.* **2021**, *537*, No. 148011.
- (20) Chernozatonskii, L. A.; Demin, V. A.; Kvashnin, D. G. Moiré Diamones: New Diamond-like Films of Semifunctionalized Twisted Graphene Layers. *J. Phys. Chem. Lett.* **2022**, *13*, 5399–5404.
- (21) Chernozatonskii, L. A.; Demin, V. A. Diamond-Like Films from Twisted Few-Layer Graphene. *JETP Lett.* **2022**, *115*, 161–166.
- (22) Tiwari, S. K.; Pandey, R.; Wang, N.; Kumar, V.; Sunday, O. J.; Bystrzejewski, M.; Zhu, Y.; Mishra, Y. K. Progress in Diamanes and Diamanoids Nanosystems for Emerging Technologies. *Adv. Sci.* **2022**, *9*, No. 2105770.
- (23) Chernozatonskii, L. A.; Demin, V. A.; Kvashnin, A. G.; Kvashnin, D. G. Diamane Quasicrystals. *Appl. Surf. Sci.* **2022**, *572*, No. 151362.
- (24) Piazza, F.; Gough, K.; Monthoux, M.; Puech, P.; Gerber, I.; Wiens, R.; Paredes, G.; Ozoria, C. Low Temperature, Pressureless Sp<sub>2</sub> to Sp<sub>3</sub> Transformation of Ultrathin, Crystalline Carbon Films. *Carbon* **2019**, *145*, 10–22.
- (25) Piazza, F.; Cruz, K.; Monthoux, M.; Puech, P.; Gerber, I. Raman Evidence for the Successful Synthesis of Diamane. *Carbon* **2020**, *169*, 129–133.
- (26) Zhu, L.; Zhang, T. Suppressed Thermal Conductivity in Fluorinated Diamane: Optical Phonon Dominant Thermal Transport. *Appl. Phys. Lett.* **2019**, *115*, 151904.
- (27) Zhu, L.; Li, W.; Ding, F. Giant Thermal Conductivity in Diamane and the Influence of Horizontal Reflection Symmetry on Phonon Scattering. *Nanoscale* **2019**, *11*, 4248–4257.
- (28) Zhang, T.; Zhu, L. Sensitive Tuning the Thermal Conductivity of Diamane via Engineering the Mass of Functional Groups. *Nanotechnology* **2020**, *31*, 435409.
- (29) Raeisi, M.; Mortazavi, B.; Podryabinkin, E. V.; Shojaei, F.; Zhuang, X.; Shapeev, A. V. High Thermal Conductivity in Semiconducting Janus and Non-Janus Diamanes. *Carbon* **2020**, *167*, 51–61.
- (30) Zheng, Z.; Zhan, H.; Nie, Y.; Xu, X.; Qi, D.; Gu, Y. Single Layer Diamond - A New Ultrathin 2D Carbon Nanostructure for Mechanical Resonator. *Carbon* **2020**, *161*, 809–815.
- (31) Hu, Y.; Li, D.; Yin, Y.; Li, S.; Ding, G.; Zhou, H.; Zhang, G. The Important Role of Strain on Phonon Hydrodynamics in Diamond-like Bi-Layer Graphene. *Nanotechnology* **2020**, *31*, 335711.
- (32) Gupta, S.; Yang, J.-H.; Yakobson, B. I. Two-Level Quantum Systems in Two-Dimensional Materials for Single Photon Emission. *Nano Lett.* **2019**, *19*, 408–414.
- (33) Qiu, D.; Wang, Q.; Cheng, S.; Gao, N.; Li, H. Electronic Structures of Two-Dimensional Hydrogenated Bilayer Diamond Films with Si Dopant and Si-V Center. *Results Phys.* **2019**, *13*, No. 102240.
- (34) Li, J.; Yin, H.; Gao, N.; Zhang, M.; Mu, J.; Gao, L.; Li, H. First-Principles Calculations for Li, P Dopants and Vacancy Defect in Ultra-Thin Hydrogenated Diamond Nanofilms: Structural, Electronic and Optical Properties. *Diam. Relat. Mater.* **2019**, *99*, No. 107526.
- (35) Gierster, L.; Vempati, S.; Stähler, J. Ultrafast Generation and Decay of a Surface Metal. *Nat. Commun.* **2021**, *12*, 978.
- (36) Elias, D. C.; Nair, R. R.; Mohiuddin, T. M. G.; Morozov, S. V.; Blake, P.; Halsall, M. P.; Ferrari, A. C.; Boukhvalov, D. W.; Katsnelson, M. I.; Geim, A. K.; Novoselov, K. S. Control of Graphene's Properties by Reversible Hydrogenation: Evidence for Graphane. *Science* **2009**, *323*, 610–613.
- (37) Luo, Z.; Yu, T.; Kim, K.; Ni, Z.; You, Y.; Lim, S.; Shen, Z.; Wang, S.; Lin, J. Thickness-Dependent Reversible Hydrogenation of Graphene Layers. *ACS Nano* **2009**, *3*, 1781–1788.
- (38) Ryu, S.; Han, M. Y.; Maultzsch, J.; Heinz, T. F.; Kim, P.; Steigerwald, M. L.; Brus, L. E. Reversible Basal Plane Hydrogenation of Graphene. *Nano Lett.* **2008**, *8*, 4597–4602.
- (39) Whitener, K. E.; Lee, W. K.; Campbell, P. M.; Robinson, J. T.; Sheehan, P. E. Chemical Hydrogenation of Single-Layer Graphene Enables Completely Reversible Removal of Electrical Conductivity. *Carbon* **2014**, *72*, 348–353.
- (40) Yang, H.; Chen, M.; Zhou, H.; Qiu, C.; Hu, L.; Yu, F.; Chu, W.; Sun, S.; Sun, L. Preferential and Reversible Fluorination of Monolayer Graphene. *J. Phys. Chem. C* **2011**, *115*, 16844–16848.
- (41) Cheng, S.-H.; Zou, K.; Okino, F.; Gutierrez, H. R.; Gupta, A.; Shen, N.; Eklund, P. C.; Sofo, J. O.; Zhu, J. Reversible Fluorination of Graphene: Evidence of a Two-Dimensional Wide Bandgap Semiconductor. *Phys. Rev. B* **2010**, *81*, No. 205435.
- (42) Cheng, L.; Jandhyala, S.; Mordi, G.; Lucero, A. T.; Huang, J.; Azcatl, A.; Addou, R.; Wallace, R. M.; Colombo, L.; Kim, J. Partially Fluorinated Graphene: Structural and Electrical Characterization. *ACS Appl. Mater. Interfaces* **2016**, *8*, 5002–5008.
- (43) Fan, K.; Liu, J.; Liu, Y.; Liu, X.; Wang, X. Phase Reversal Behavior on Two-Dimension Plane of Fluorinated Graphene during Defluorination. *Carbon* **2021**, *183*, 660–671.

- (44) Erohin, S. V.; Ruan, Q.; Sorokin, P. B.; Yakobson, B. I. Nano-Thermodynamics of Chemically Induced Graphene–Diamond Transformation. *Small* **2020**, *16*, No. 2004782.
- (45) Hedin, L. New Method for Calculating the One-Particle Green's Function with Application to the Electron-Gas Problem. *Phys. Rev.* **1965**, *139*, A796–A823.
- (46) Bader, R. F. W. Atoms in Molecules: A Quantum Theory; *International Series of Monographs on Chemistry*; Oxford University Press: Oxford, New York, 1994.
- (47) Tantardini, C.; Ceresoli, D.; Benassi, E. Source Function and Plane Waves: Toward Complete Bader Analysis. *J. Comput. Chem.* **2016**, *37*, 2133–2139.
- (48) Tikhomirova, K. A.; Tantardini, C.; Sukhanova, E. V.; Popov, Z. I.; Evlashin, S. A.; Tarkhov, M. A.; Zhdanov, V. L.; Dudin, A. A.; Oganov, A. R.; Kvashnin, D. G.; Kvashnin, A. G. Exotic Two-Dimensional Structure: The First Case of Hexagonal NaCl. *J. Phys. Chem. Lett.* **2020**, *11*, 3821–3827.
- (49) Tantardini, C.; Kvashnin, A. G.; Gatti, C.; Yakobson, B. I.; Gonze, X. Computational Modeling of 2D Materials under High Pressure and Their Chemical Bonding: Silicene as Possible Field-Effect Transistor. *ACS Nano* **2021**, *15*, 6861–6871.
- (50) Tran, F.; Blaha, P. Accurate Band Gaps of Semiconductors and Insulators with a Semilocal Exchange-Correlation Potential. *Phys. Rev. Lett.* **2009**, *102*, No. 226401.
- (51) Tantardini, C.; Gonze, X. Band Gap Bowing and Spectral Width of Ga(1-x)InxN Alloys for Modelling Light Emitting Diodes. *Phys. B: Condens. Matter* **2021**, *625*, No. 413481.
- (52) Waroquiers, D.; Lherbier, A.; Miglio, A.; Stankovski, M.; Ponc  , S.; Oliveira, M. J. T.; Giantomassi, M.; Rignanese, G.-M.; Gonze, X. Band Widths and Gaps from the Tran-Blaha Functional: Comparison with Many-Body Perturbation Theory. *Phys. Rev. B* **2013**, *87*, No. 075121.
- (53) Borlido, P.; Aull, T.; Huran, A. W.; Tran, F.; Marques, M. A. L.; Botti, S. Large-Scale Benchmark of Exchange–Correlation Functionals for the Determination of Electronic Band Gaps of Solids. *J. Chem. Theory Comput.* **2019**, *15*, 5069–5079.
- (54) Helmholtz, H. Ueber Einige Gesetze Der Vertheilung Elektrischer Str  me in K  rperlichen Leitern Mit Anwendung Auf Die Thierisch-Elektrischen Versuche. *Ann. Phys.* **1853**, *165*, 211–233.
- (55) Ehrenstein, G.; Gilbert, D. L. Evidence for Membrane Surface from Measurement of Potassium Kinetics as a Function of External Divalent Cation Concentration. *Biophys. J.* **1973**, *13*, 495–497.
- (56) Grahame, D. C. The Electrical Double Layer and the Theory of Electrocapillarity. *Chem. Rev.* **1947**, *41*, 441–501.
- (57) Stern, O. Zur Theorie Der Elektrolytischen Doppelschicht. *Z. Elektrochem. Angew. Phys. Chem.* **1924**, *30*, 508–516.
- (58) Pauling, L. The Nature Of The Chemical Bond. IV. The Energy Of Single Bonds And The Relative Electronegativity Of Atoms. *J. Am. Chem. Soc.* **1932**, *54*, 3570–3582.
- (59) Dederichs, P. H.; Bl  gel, S.; Zeller, R.; Akai, H. Ground States of Constrained Systems: Application to Cerium Impurities. *Phys. Rev. Lett.* **1984**, *53*, 2512–2515.
- (60) Kaduk, B.; Kowalczyk, T.; Van Voorhis, T. Constrained Density Functional Theory. *Chem. Rev.* **2012**, *112*, 321–370.
- (61) Gonze, X.; Seddon, B.; Elliott, J. A.; Tantardini, C.; Shapeev, A. V. Constrained Density Functional Theory: A Potential-Based Self-Consistency Approach. *J. Chem. Theory Comput.* **2022**, *18*, 6099–6110.
- (62) Tantardini, C.; Oganov, A. R. Thermochemical Electronegativities of the Elements. *Nat. Commun.* **2021**, *12*, 2087.
- (63) *Diatom Spectral Database*; NIST 2009.
- (64) Bader, R. F. W.; Larouche, A.; Gatti, C.; Carroll, M. T.; MacDougall, P. J.; Wiberg, K. B. Properties of Atoms in Molecules: Dipole Moments and Transferability of Properties. *J. Chem. Phys.* **1987**, *87*, 1142–1152.
- (65) Gatti, C.; Saunders, V. R.; Roetti, C. Crystal Field Effects on the Topological Properties of the Electron Density in Molecular Crystals: The Case of Urea. *J. Chem. Phys.* **1994**, *101*, 10686–10696.
- (66) Hamann, D. R. Optimized Norm-Conserving Vanderbilt Pseudopotentials. *Phys. Rev. B* **2013**, *88*, No. 085117.
- (67) van Setten, M. J.; Giantomassi, M.; Bousquet, E.; Verstraete, M. J.; Hamann, D. R.; Gonze, X.; Rignanese, G.-M. The PseudoDojo: Training and Grading a 85 Element Optimized Norm-Conserving Pseudopotential Table. *Comput. Phys. Commun.* **2018**, *226*, 39–54.
- (68) Perdew, J. P.; Burke, K.; Ernzerhof, M. Generalized Gradient Approximation Made Simple. *Phys. Rev. Lett.* **1997**, *78*, 1396–1396.
- (69) Gonze, X.; Jollet, F.; Abreu Araujo, F.; Adams, D.; Amadon, B.; Applencourt, T.; Audouze, C.; Beuken, J.-M.; Bieder, J.; Bokhanchuk, A.; Bousquet, E.; Bruneval, F.; Caliste, D.; C  te, M.; Dahm, F.; Da Piev  , F.; Delaveau, M.; Di Gennaro, M.; Dorado, B.; Espejo, C.; Geneste, G.; Genovese, L.; Gerossier, A.; Giantomassi, M.; Gillet, Y.; Hamann, D. R.; He, L.; Jomard, G.; Laflamme Janssen, J.; Le Roux, S.; Levitt, A.; Lherbier, A.; Liu, F.; Luka  vi  , I.; Martin, A.; Martins, C.; Oliveira, M. J. T.; Ponc  , S.; Pouillon, Y.; Rangel, T.; Rignanese, G.-M.; Romero, A. H.; Rousseau, B.; Rubel, O.; Shukri, A. A.; Stankovski, M.; Torrent, M.; Van Setten, M. J.; Van Troeye, B.; Verstraete, M. J.; Waroquiers, D.; Wiktor, J.; Xu, B.; Zhou, A.; Zwanziger, J. W. Recent Developments in the ABINIT Software Package. *Comput. Phys. Commun.* **2016**, *205*, 106–131.
- (70) Gonze, X.; Amadon, B.; Antonius, G.; Arnardi, F.; Baguet, L.; Beuken, J.-M.; Bieder, J.; Bottin, F.; Bouchet, J.; Bousquet, E.; Brouwer, N.; Bruneval, F.; Brunin, G.; Cavignac, T.; Charraud, J.-B.; Chen, W.; C  te, M.; Cottenier, S.; Denier, J.; Geneste, G.; Ghosez, P.; Giantomassi, M.; Gillet, Y.; Gingras, O.; Hamann, D. R.; Hautier, G.; He, X.; Helbig, N.; Holzwarth, N.; Jia, Y.; Jollet, F.; Lafargue-Dit-Hauret, W.; Lejaeghere, K.; Marques, M. A. L.; Martin, A.; Martins, C.; Miranda, H. P. C.; Naccarato, F.; Persson, K.; Petretto, G.; Planes, V.; Pouillon, Y.; Prokhorenko, S.; Ricci, F.; Rignanese, G.-M.; Romero, A. H.; Schmitt, M. M.; Torrent, M.; van Setten, M. J.; Van Troeye, B.; Verstraete, M. J.; Z  rah, G.; Zwanziger, J. W. The Abinitproject: Impact, Environment and Recent Developments. *Comput. Phys. Commun.* **2020**, *248*, No. 107042.
- (71) Broyden, C. G. The Convergence of a Class of Double-Rank Minimization Algorithms 1. General Considerations. *IMA J. Appl. Math.* **1970**, *6*, 76–90.
- (72) Goldfarb, D. A Family of Variable-Metric Methods Derived by Variational Means. *Math. Comput.* **1970**, *24*, 23–26.
- (73) Shanno, D. F. Conditioning of Quasi-Newton Methods for Function Minimization. *Math. Comput.* **1970**, *24*, 647–656.
- (74) Steihaug, T. *Practical Methods of Optimization Volume 1 : Unconstrained Optimization*; 1982.
- (75) Hartwigsen, C.; Goedecker, S.; Hutter, J. Relativistic Separable Dual-Space Gaussian Pseudopotentials from H to Rn. *Phys. Rev. B* **1998**, *58*, 3641–3662.
- (76) Ismail-Beigi, S. Truncation of Periodic Image Interactions for Confined Systems. *Phys. Rev. B* **2006**, *73*, No. 233103.
- (77) Shaltaf, R.; Rignanese, G.-M.; Gonze, X.; Giustino, F.; Pasquarello, A. Band Offsets at the Si/SiO<sub>2</sub> Interface from Many-Body Perturbation Theory. *Phys. Rev. Lett.* **2008**, *100*, No. 186401.
- (78) Neugebauer, J.; Scheffler, M. Adsorbate-Substrate and Adsorbate-Adsorbate Interactions of Na and K Adlayers on Al(111). *Phys. Rev. B* **1992**, *46*, 16067–16080.
- (79) Baldereschi, A.; Baroni, S.; Resta, R. Band Offsets in Lattice-Matched Heterojunctions: A Model and First-Principles Calculations for GaAs/AlAs. *Phys. Rev. Lett.* **1988**, *61*, 734–737.
- (80) Jiang, H. Electronic Band Structures of Molybdenum and Tungsten Dichalcogenides by the GW Approach. *J. Phys. Chem. C* **2012**, *116*, 7664–7671.
- (81) Kendall, R. A.; Dunning, T. H., Jr.; Harrison, R. J. Electron Affinities of the First-row Atoms Revisited. Systematic Basis Sets and Wave Functions. *J. Chem. Phys.* **1992**, *96*, 6796–6806.
- (82) Peterson, K. A.; Figgen, D.; Goll, E.; Stoll, H.; Dolg, M. Systematically Convergent Basis Sets with Relativistic Pseudopotentials. II. Small-Core Pseudopotentials and Correlation Consistent Basis Sets for the Post-d Group 16–18 Elements. *J. Chem. Phys.* **2003**, *119*, 11113–11123.

- (83) Peterson, K. A.; Yousaf, K. E. Molecular Core-Valence Correlation Effects Involving the Post-d Elements Ga–Rn: Benchmarks and New Pseudopotential-Based Correlation Consistent Basis Sets. *J. Chem. Phys.* **2010**, *133*, 174116.
- (84) Frisch, M. J.; Trucks, G. W.; Schlegel, H. B.; Scuseria, G. E.; Robb, M. A.; Cheeseman, J. R.; Scalmani, G.; Barone, V.; Petersson, G. A.; Nakatsuji, H.; Li, X.; Caricato, M.; Marenich, A. V.; Bloino, J.; Janesko, B. G.; Gomperts, R.; Mennucci, B.; Hratchian, H. P.; Ortiz, J. V.; Izmaylov, A. F.; Sonnenberg, J. L.; Williams-Young, D.; Ding, F.; Lipparini, F.; Egidi, F.; Goings, J.; Peng, B.; Petrone, A.; Henderson, T.; Ranasinghe, D.; Zakrzewski, V. G.; Gao, J.; Rega, N.; Zheng, G.; Liang, W.; Hada, M.; Ehara, M.; Toyota, K.; Fukuda, R.; Hasegawa, J.; Ishida, M.; Nakajima, T.; Honda, Y.; Kitao, O.; Nakai, H.; Vreven, T.; Throssell, K.; Montgomery, J. A., Jr.; Peralta, J. E.; Ogliaro, F.; Bearpark, M. J.; Heyd, J. J.; Brothers, E. N.; Kudin, K. N.; Staroverov, V. N.; Keith, T. A.; Kobayashi, R.; Normand, J.; Raghavachari, K.; Rendell, A. P.; Burant, J. C.; Iyengar, S. S.; Tomasi, J.; Cossi, M.; Millam, J. M.; Klene, M.; Adamo, C.; Cammi, R.; Ochterski, J. W.; Martin, R. L.; Morokuma, K.; Farkas, O.; Foresman, J. B.; Fox, D. J. *Gaussian 16 Revision C.01*; 2016.
- (85) Otero-de-la-Roza, A.; Johnson, E. R.; Lúaña, V. Critic2: A Program for Real-Space Analysis of Quantum Chemical Interactions in Solids. *Comput. Phys. Commun.* **2014**, *185*, 1007–1018.
- (86) Momma, K.; Izumi, F. VESTA 3 for Three-Dimensional Visualization of Crystal, Volumetric and Morphology Data. *J. Appl. Crystallogr.* **2011**, *44*, 1272–1276.

## □ Recommended by ACS

### Understanding the Evolution of the Structure and Electrical Properties during Crystallization of $\text{Li}_{1.5}\text{Al}_{0.5}\text{Ge}_{1.5}(\text{PO}_4)_3$ and $\text{Li}_{1.5}\text{Sc}_{0.17}\text{Al}_{0.33}\text{Ge}_{1.5}(\text{PO}_4)_3$ NASICON -Type Glass

Jeferson A. Dias, Younès Messaddeq, et al.

MARCH 22, 2023

THE JOURNAL OF PHYSICAL CHEMISTRY C

READ ▶

### On the Optical Properties of Diamino-Pillared Graphene Architectures

Emilia Papasouli, Panagiotis Karamanis, et al.

MARCH 29, 2023

THE JOURNAL OF PHYSICAL CHEMISTRY C

READ ▶

### Enhancement in High-Field $J_c$ Properties and the Flux Pinning Mechanism of ZnO-Buffered $\text{MgB}_2$ Films

Rico Pratama Putra, Byeongwon Kang, et al.

MARCH 15, 2023

ACS OMEGA

READ ▶

### Chemical Vapor Deposition of Monolayer $\text{MoS}_2$ on Chemomechanically Polished N-Polar GaN for Future 2D/3D Heterojunction Optoelectronics

Rohan Sengupta, Spyridon Pavlidis, et al.

MARCH 24, 2023

ACS APPLIED NANO MATERIALS

READ ▶

Get More Suggestions >